# Dual fermion dynamical cluster approach for strongly correlated systems

S.-X. Yang,[1] H. Fotso,[1] H. Hafermann,[2] K.-M. Tam,[1] J. Moreno,[1] T. Pruschke,[3] and M. Jarrell[1]
[1]*Department of Physics and Astronomy, Louisiana State University, Baton Rouge, Louisiana 70803, USA*
[2]*Centre de Physique Théorique, École Polytechnique, CNRS, FR-91128 Palaiseau Cedex, France*
[3]*Department of Physics, University of Göttingen, GE-37077 Göttingen, Germany*
(Received 10 May 2011; revised manuscript received 2 September 2011; published 11 October 2011)

We have designed a multiscale approach for strongly correlated systems by combining the dynamical cluster approximation (DCA) and the recently introduced dual fermion formalism. This approach employs an exact mapping from a real lattice to a DCA cluster of linear size $L_c$ embedded in a dual fermion lattice. Short-length-scale physics is addressed by the DCA cluster calculation, while longer-length-scale physics is addressed diagrammatically using dual fermions. The bare and dressed dual fermionic Green functions scale as $\mathcal{O}(1/L_c)$, so perturbation theory on the dual lattice converges very quickly, e.g., the dual Fermion self-energy calculated with simple second-order perturbation theory is of order $\mathcal{O}(1/L_c^3)$ with third-order and three-body corrections down by an additional factor of $\mathcal{O}(1/L_c)$.

DOI: 10.1103/PhysRevB.84.155106 PACS number(s): 71.27.+a, 71.10.Fd

## I. INTRODUCTION

Dynamical mean-field theory[1–3] has been remarkably successful at capturing the physics of strongly correlated systems dominated by spatially local correlations. Successes include the description of the Mott transition in the Hubbard model, screening effects in the periodic Anderson model as well as the description of correlation effects in realistic systems.[4–6]

Since the introduction of the dynamical mean-field approximation (DMFA), there have been a number of attempts to develop formal extensions around the DMFA that incorporate nonlocal corrections. These include cluster extensions of the DMFA, such as the dynamical cluster approximation (DCA)[7–9] or the cellular dynamical mean-field theory (CDMFT),[10] and multiscale approximations where the DMFA or DCA vertices are used to parametrize two-particle field theories and longer-ranged correlations can thus be captured.[11–13] One of the main limitations of these theories is that they converge slowly with the linear cluster size $L_c$, especially for the calculation of transition temperatures.

The dual fermion formalism[14–16] is however, distinctly different from other cluster extensions of the DMFA. In the dual fermion formalism, the lattice action is first mapped onto a dual fermion action where the interaction vertices are the $n$-body reducible vertices of the cluster. This mapping is exact, so the dual fermion formalism provides a complete and exact formalism for the lattice problem. Thus far, the dual fermion formalism has only been explored using the DMFA or the CDMFT as cluster solvers.[17] However, the CDMFT has the disadvantage in this context that it violates translational invariance, so that the CDMFT vertices are rank-four tensors in the spatial or momentum indices, which are too large to be stored and manipulated on most computers, especially for large clusters. Thus in this manuscript, we propose the dual fermion dynamical cluster approach (DFDCA), within which the long-ranged correlations can be systematically incorporated through the dual fermion lattice calculation. Since the DCA preserves the translational invariance of the lattice system, the DCA two-body vertices are rank-three tensors, which, for modest cluster sizes, will fit in the memory of modern computers. Another difference, which we will discuss in detail, is that the small parameter for the DFDCA is the dual fermion single-particle Green function, which scales as $G_d \sim \mathcal{O}(1/L_c)$ with $L_c$ being the linear cluster size. As a result, perturbation theory on the dual fermion lattice converges very quickly. Simple second-order perturbation theory on the dual fermion lattice already yields a dual fermion self-energy of order $\mathcal{O}(1/L_c^3)$ with two-body and three-body corrections down by an additional factor of $\mathcal{O}(1/L_c)$. Higher-order approximations are also possible, since, e.g., the three-body vertex corrections to the DFDCA self-energy are small, $\mathcal{O}(1/L_c^4)$. Therefore the resulting DFDCA formalism converges very quickly with increasing cluster size with corrections to the self-energy no larger than $\mathcal{O}(1/L_c^4)$.

## II. MAPPING THE DCA FORMALISM TO DUAL FERMIONS

We will derive the DFDCA formalism with the example of the Hubbard model. Its Hamiltonian is

$$H = -\sum_{\langle ij\rangle} t_{ij}(c_{i\sigma}^{\dagger}c_{j\sigma} + \text{H.c.}) + U\sum_{i}(n_{i\uparrow} - 1/2)(n_{i\downarrow} - 1/2), \quad (1)$$

where $t_{ij}$ is the matrix of hopping integrals, $c_{i\sigma}^{(\dagger)}$ is the annihilation (creation) operator for electrons on lattice site $i$ with spin $\sigma$, $n_{i\sigma} = c_{i\sigma}^{\dagger}c_{i\sigma}$, and $U$ is the intra-atomic repulsion.

The DMFA, and its cluster extensions such as the DCA, are based upon the common idea of embedding a cluster in a lattice. We assume that the cluster, of size $N_c = L_c^D$, dimensionality $D$, sites labeled by $I$ and wave vectors $K$, is embedded in a large but finite-sized lattice of size $N$ with sites $i$ and wave vectors $k$. In the DCA, the reciprocal space of the lattice is divided into $N_c$ cells of identical geometry and linear size $\Delta k$. The cell centers are labeled by $K$, and the points surrounding $K$ within the coarse-graining cell are

 

labeled with $\tilde{k}$. We will also invoke a dual space lattice, which is of the same size and geometry as the real lattice.

The action for this model is

$$S[c^*,c] = -\sum_{\omega,k,\sigma} c^*_{\omega,k,\sigma}[(i\omega+\mu)\mathbf{1} - h_k]c_{\omega,k,\sigma} + \sum_i S_{\rm loc}[c_i^*,c_i], \tag{2}$$

where $S_{\rm loc}[c_i^*,c_i]$ is the local part of the action including the Hubbard interaction term, $c_i^*$ and $c_i$ are now Grassmann numbers corresponding to creation and annihilation operators on the lattice, $\mu$ is the chemical potential, $h_k$ is the lattice bare dispersion, and $\omega = (2n+1)\pi T$ are the Matsubara frequencies. Decomposing the wave vector according to $k = K + \tilde{k}$, the lattice action becomes

$$S[c^*,c] = \sum_i S_{\rm loc}[c_i^*,c_i] - \sum_{\omega,K,\tilde{k},\sigma} c^*_{\omega,K+\tilde{k},\sigma}[(i\omega+\mu)\mathbf{1} - h_{K+\tilde{k}}]c_{\omega,K+\tilde{k},\sigma}. \tag{3}$$

The goal is to express this action in terms of the DCA cluster problem[18]

$$S_{\rm cluster}[\overline{c}^*,\overline{c}] = \sum_I S_{\rm loc}[\overline{c}_I^*,\overline{c}_I] - \sum_{\omega,K,\sigma} \overline{c}^*_{\omega,K,\sigma}[(i\omega+\mu)\mathbf{1} - \overline{h}_K - \Delta(K,i\omega)]\overline{c}_{\omega,K,\sigma}, \tag{4}$$

where $\overline{c}_I^*$ and $\overline{c}_I$ are now Grassmann numbers corresponding to creation and annihilation operators on the DCA cluster, and $\Delta(K,i\omega)$ is the cluster hybridization function. To this end, we add and subtract the hybridization function and coarse-grained dispersion, i.e.,

$$\sum_{\omega,K,\tilde{k},\sigma} c^*_{\omega,K+\tilde{k},\sigma}[\overline{h}_K + \Delta(K,i\omega)]c_{\omega,K+\tilde{k},\sigma} = \frac{N}{N_c}\sum_{\omega,K,\sigma} \overline{c}^*_{\omega,K,\sigma}[\overline{h}_K + \Delta(K,i\omega)]\overline{c}_{\omega,K,\sigma}, \tag{5}$$

where the last line follows from the DCA coarse-graining identity

$$\overline{c}^*_{\omega,K,\sigma}\overline{c}_{\omega,K,\sigma} \equiv \frac{N_c}{N}\sum_{\tilde{k}} c^*_{\omega,K+\tilde{k},\sigma}c_{\omega,K+\tilde{k},\sigma} \tag{6}$$

and the coarse-grained dispersion is given by

$$\overline{h}_K = \frac{N_c}{N}\sum_{\tilde{k}} h_{K+\tilde{k}}. \tag{7}$$

The DCA coarse-graining identity preserves the fermionic Lie algebra, despite the fact that it is not a canonical transformation,

$$\{\overline{c}^\dagger_{K,\sigma},\overline{c}_{K',\sigma'}\} = \frac{N_c}{N}\sum_{\tilde{k}}\{c^\dagger_{K+\tilde{k},\sigma},c_{K'+\tilde{k},\sigma'}\} = \delta_{K\sigma,K'\sigma'}, \tag{8}$$

where the last step follows since the coarse-graining cells surrounding $K$ and $K'$ have the same geometry and contain the same number of states which, therefore, may be labeled with the same $\tilde{k}$. We then obtain

$$S[c^*,c] = \sum_i S_{\rm loc}[c_i^*,c_i] - \sum_{\omega,K,\tilde{k},\sigma} c^*_{\omega,K+\tilde{k},\sigma}[(i\omega+\mu)\mathbf{1} - \overline{h}_K - \Delta(K,i\omega)]c_{\omega,K+\tilde{k},\sigma} - \sum_{\omega,k,\sigma} c^*_{\omega,k,\sigma}[\Delta(M(k),i\omega) + \overline{h}_{M(k)} - h_k]c_{\omega,k,\sigma}. \tag{9}$$

In the third line of this equation, we have introduced the function $M(k)$, which maps the momentum $k$ in the DCA momentum cell to the cluster momentum contained in that cell. Coarse graining the first and the second terms on the right-hand side of the above equation yields the cluster action (4). Since the latter is independent of $\tilde{k}$, we may write

$$S[c^*,c] = \sum_{\tilde{k}} S_{\rm cluster}[\overline{c}^*,\overline{c}] - \sum_{\omega,k,\sigma} c^*_{\omega,k,\sigma}[\Delta(M(k),i\omega) + \overline{h}_{M(k)} - h_k]c_{\omega,k,\sigma}. \tag{10}$$

Again, up to this point, we have only rearranged terms and employed an identity, which defines $\overline{c}$. No approximation has been made.

The dual fermions are now introduced by means of the following Gaussian identity:

$$\int \exp(-f^*_\alpha a_{\alpha\beta}f_\beta - f^*_\alpha b_{\alpha\beta}c_\beta - c^*_\alpha b_{\alpha\beta}f_\beta)\Pi_\gamma df^*_\gamma df_\gamma = \det(a)\exp[c^*_\alpha(ba^{-1}b)_{\alpha\beta}c_\beta] \tag{11}$$

for Grassmann variables in the path-integral representation for the partition function,

$$\int \exp(-S[c^*,c])\mathcal{D}[c^*,c]. \tag{12}$$

To be specific, we choose the (diagonal) matrices according to

$$a_{\omega,k,\sigma} = \bar{g}^{-2}(M(k),i\omega)[\Delta(M(k),i\omega) + \overline{h}_{M(k)} - h_k]^{-1}, \quad b_{\omega,k,\sigma} = \bar{g}^{-1}(M(k),i\omega), \tag{13}$$

where $\bar{g}$ is the single-particle Green function calculated on the DCA cluster. Applying the above identity to the second term in Eq. (10), yields

$$\sum_{\omega,k,\sigma}\frac{f^*_{\omega,k,\sigma}\,f_{\omega,k,\sigma}}{\bar{g}^2(M(k),i\omega)[\Delta(M(k),i\omega) + \overline{h}_{M(k)} - h_k]} + \sum_{\omega,k,\sigma}[f^*_{\omega,k,\sigma}\bar{g}^{-1}(M(k),i\omega)c_{\omega,k,\sigma} + \text{H.c.}]. \tag{14}$$

The essential observation now is that, since $\bar{g}^{-1}(M(k),i\omega) \equiv \bar{g}^{-1}(K,i\omega)$ is independent of $\tilde{k}$, the second line of Eq. (14) may be coarse grained using again the DCA coarse-graining identity

$$\overline{f}^*_{\omega,K,\sigma}\overline{c}_{\omega,K,\sigma} \equiv \frac{N_c}{N}\sum_{\tilde{k}} f^*_{\omega,K+\tilde{k},\sigma}c_{\omega,K+\tilde{k},\sigma}. \tag{15}$$

As a consequence, the lattice action, Eq. (10), can be expressed in the form

$$S[c^*,c;f^*,f] = \sum_{\tilde{k}} S_{\rm restr}[\overline{c}^*,\overline{c};\overline{f}^*,\overline{f}] + \sum_{\omega,K,\tilde{k},\sigma} \frac{f^*_{\omega,K+\tilde{k},\sigma}\, f_{\omega,K+\tilde{k},\sigma}}{\bar{g}^2(K,i\omega)[\Delta(K,i\omega)+\overline{h}_K - h_k]}, \tag{16}$$

where

$$S_{\rm restr}[\overline{c}^*,\overline{c};\overline{f}^*,\overline{f}] = S_{\rm cluster}[\overline{c}^*,\overline{c}] + \sum_{\omega,K,\sigma} [\overline{f}^*_{\omega,K,\sigma}\bar{g}^{-1}(K,i\omega)\overline{c}_{\omega,K,\sigma} + \text{H.c.}] \tag{17}$$

is the action restricted to the cluster.

The transformation to dual fermions is completed by integrating out the fermionic degrees of freedom corresponding to $\overline{c}$ and $\overline{c}^*$. Since $S_{\rm restr}$ is independent of $\tilde{k}$, this can be done individually for each cluster

$$\frac{1}{Z_{\rm cluster}} \int \exp(-S_{\rm restr}[\overline{c}^*,\overline{c};\overline{f}^*,\overline{f}])\mathcal{D}[\overline{c}^*,\overline{c}] = \exp\left\{ -\sum_{\omega,K,\sigma} \overline{f}^*_{\omega,K,\sigma}\bar{g}^{-1}(K,i\omega)\overline{f}_{\omega,K,\sigma} - V[\overline{f}^*,\overline{f}] \right\}. \tag{18}$$

Equation (18) defines the dual potential that can be obtained by expanding both sides and comparing the resulting expressions order by order. It is given by[19]

$$V[\overline{f}^*,\overline{f}] = \frac{1}{4} \sum_{KK'Q} \sum_{\omega\omega'\nu} \sum_{\sigma_1,\sigma_2,\sigma_3,\sigma_4} \gamma_{\sigma_1,\sigma_2,\sigma_3,\sigma_4}(K,K',Q;i\omega,i\omega',i\nu) \times \overline{f}^*_{\omega+\nu,K+Q,\sigma_1}\overline{f}_{\omega,K,\sigma_2}\overline{f}^*_{\omega',K',\sigma_3}\overline{f}_{\omega'+\nu,K'+Q,\sigma_4} + \ldots, \tag{19}$$

where $\gamma$ is the full (reducible) vertex of the cluster quantum impurity model, and the higher-order contributions involve the $n$ body (for $n > 2$) reducible vertices as the bare interaction. Integrating out the lattice fermions results in an action that depends only on the dual fermion degrees of freedom given by

$$S_d[f^*,f] = -\sum_{k\omega\sigma} f^*_{\omega k\sigma} G^0_d(k,i\omega)^{-1} f_{\omega k\sigma} + \sum_{\tilde{k}} V[\overline{f}^*,\overline{f}], \tag{20}$$

where $G^0_d$ is the bare dual Green function defined by

$$G^0_d(k,i\omega) = -\frac{\overline{g}(K,i\omega)^2}{\overline{g}(K,i\omega) + (\Delta(K,i\omega)+\overline{h}_K - h_k)^{-1}}. \tag{21}$$

This quantity together with the dual potential $V[\overline{f}^*,\overline{f}]$ provides sufficient input for a many-body diagrammatic perturbation calculation on the dual lattice. Note that besides the DCA coarse-graining process introduced here, the above derivation is a natural generalization of the dual fermion DMFA formulation of Rubtsov *et al.*[14]

### A. Self-consistency condition

In rewriting the lattice action in terms of the cluster impurity model in the above derivation, the DCA hybridization function has been added and subtracted and hence is an arbitrary quantity. In order to fix this quantity, we impose the condition

$$G^0_d(K,i\omega) = \frac{N_c}{N} \sum_{\tilde{k}} G^0_d(K+\tilde{k},i\omega) \stackrel{!}{=} 0. \tag{22}$$

To appreciate the consequences of this condition, first consider the DCA lattice Green function

$$G^{-1}_{\rm DCA}(K+\tilde{k},i\omega) = (i\omega+\mu)\mathbf{1} - h_{K+\tilde{k}} - \Sigma_c(K,i\omega), \tag{23}$$

which can be expressed in terms of the cluster Green function

$$\bar{g}^{-1}(K,i\omega) = (i\omega+\mu)\mathbf{1} - \overline{h}_K - \Sigma_c(K,i\omega) - \Delta_c(K,i\omega), \tag{24}$$

as

$$G^{-1}_{\rm DCA}(K+\tilde{k},i\omega) = \bar{g}^{-1}(K,i\omega) + \Delta_c(K,i\omega) + \overline{h}_K - h_{K+\tilde{k}}. \tag{25}$$

Using the last expression, one may straightforwardly derive the following identity relating the DCA lattice Green function to the bare dual Green function

$$G^{d,0}(K+\tilde{k},i\omega) = G_{\rm DCA}(K+\tilde{k},i\omega) - \bar{g}(K,i\omega). \tag{26}$$

Hence the above condition (22) is equivalent to requiring that the coarse-grained DCA lattice Green function be equal to the Green function of the cluster impurity model. This is exactly the DCA self-consistency condition. The DCA solution is therefore obtained if no diagrammatic corrections are taken into account and the hybridization is determined such that the condition (22) holds. Consequently, we have a perturbation theory around the DCA as the starting point. While the DCA solution only depends on the cluster momentum K, the dependence on $\tilde{k}$ can be introduced by solving the dual problem perturbatively.

### B. Scaling of the dual fermion DCA approach with cluster size

The bare dual Green function is given by Eq. (21). If we introduce the linear cluster size $L_c$ through $N_c = L_c^D$, one finds that the term $[\Delta(K,i\omega)+\overline{h}_K - h_k] \sim \mathcal{O}(1/L_c)$. The small nature of this term for large $L_c$ should ensure rapid convergence of the DFDCA. In particular, we then have

$$G^0_d(k,i\omega) = -\overline{g}(K,i\omega)[\Delta(K,i\omega)+\overline{h}_K - h_k]\overline{g}(K,i\omega) + \mathcal{O}(1/L_c^2), \tag{27}$$

i.e., the bare dual Green function also scales like

$$G^0_d(k,i\omega) \sim \mathcal{O}(1/L_c). \tag{28}$$

However, at points of high symmetry, where $\overline{h}_K - h_k \sim \mathcal{O}(1/L_c^2)$, $G^0_d(k,i\omega)$ will fall more quickly than $\mathcal{O}(1/L_c)$.

To illustrate the typical scaling behavior of the bare dual Green function, we plot in Fig. 1, as a function of $1/L_c$, the ratio of $|G^0_d(k,i\omega = i\pi T,L_c)|$ averaged over $k$ to the average $|G^0_d(k,i\omega = i\pi T,L_c = 1)|$. We also plot the average of the ratios. The former initially falls more quickly than $\mathcal{O}(1/L_c)$, while the latter displays a slower initial slope. However, for

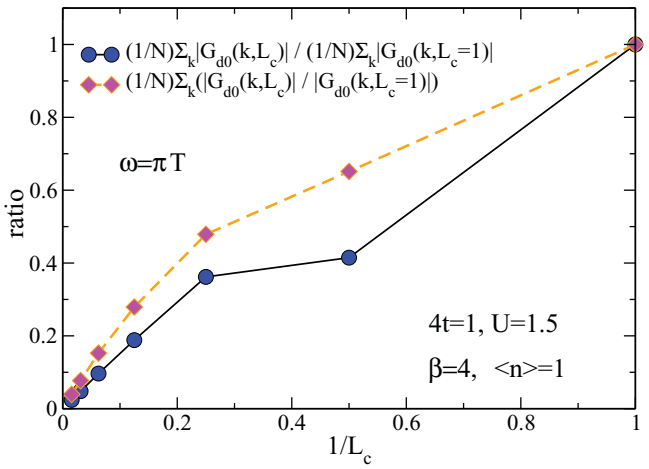


FIG. 1. (Color online) Scaling plot for the bare dual Green function. Here, we have used the 1D Hubbard model to analyze its scaling behavior. Except for very small $L_c$ values, the two ratios scale linearly according to Eq. (28).

$L_c \geqslant 4$, both fall roughly linearly in $1/L_c$. This behavior is found to be independent of temperature (not shown), since it is a purely algebraic effect.

Applying the standard tools to the dual fermion action, one obtains the formal expression

$$G_d(k,i\omega) = G_d^0(k,i\omega) + G_d^0(k,i\omega)T_d(k,i\omega)G_d^0(k,i\omega), \quad (29)$$

for the full dual fermion Green function $G_d(k,i\omega)$, where the reducible self-energy or scattering matrix $T_d(k,i\omega)$ of the dual system is introduced. We will show later, that $T_d(k,i\omega)$ will be at most of order $\mathcal{O}(1/L_c^3)$, and we can infer the scaling

$$G_d(k,i\omega) \sim \mathcal{O}(1/L_c) \quad (30)$$

for the full dual fermion Green function too.

Once the dual fermion Green function is known, one can reconstruct the real lattice Green function as

$$G(k,i\omega) = \overline{g}(K,i\omega)^{-2}[\Delta(K,i\omega) + \overline{h}_K - h_k]^{-2}G_d(k,i\omega) + [\Delta(K,i\omega) + \overline{h}_K - h_k]^{-1}. \quad (31)$$

Since $G(k,i\omega)$ is the Green function of the real lattice, it should scale as

$$G(k,i\omega) \sim \mathcal{O}(1) \quad (32)$$

with respect to any length scale. On the other hand, for the two terms on the right-hand side in Eq. (31), we find

$$\overline{g}(K,i\omega)^{-2}[\Delta(K,i\omega) + \overline{h}_K - h_k]^{-2}G_d(k,i\omega) \sim \mathcal{O}(L_c) \quad (33)$$

and

$$[\Delta(K,i\omega) + \overline{h}_K - h_k]^{-1} \sim \mathcal{O}(L_c)\,. \quad (34)$$

Thus the two $\mathcal{O}(L_c)$ terms must cancel each other. To verify this requirement, we insert the zeroth order contribution of the dual Green function into the original Green function, and after some algebra we indeed obtain

$$G(k,i\omega) \sim \overline{g}(K,i\omega) \sim \mathcal{O}(1), \quad (35)$$

with a correction given by

$$\Delta G(k,i\omega) \sim T_d(k,i\omega). \quad (36)$$

Therefore the correction to the real Green function through the dual fermion approach scales the same way as the dual self-energy.

Presently, the dual potential, Eq. (19), still contains an infinite hierarchy of vertices. The previous discussion now provides a very important insight into the contributions of these vertices to a perturbative expansion: each $n$ body diagrammatic insertion will involve a vertex and $n$ Green function lines. In the parameter region away from a critical point, the dual potential will be of order $\mathcal{O}(1)$. As noted before, the dual Green function is of order $\mathcal{O}(1/L_c)$, i.e., each dual space diagrammatic insertion is of order $\mathcal{O}(1/L_c^2)$ when it involves the two-body dual space interaction, of order $\mathcal{O}(1/L_c^3)$ for the three-body interaction, and so on. This means that the two-body contribution to $V$, explicitly shown in Eq. (19), will actually dominate and low-order perturbation theory will be sufficient to accurately capture the corrections to the DCA from the dual fermion lattice.

### C. Mapping back from the dual fermion to the real lattice

The relation of the real fermion Green function to the dual Green function has been been established in Eq. (31). This is an exact relation which follows by taking the functional derivative of two equivalent partition functions. They are linked through the same Gaussian identity that has been used to introduce the dual fermions [Eq. (11)]. Higher-order derivatives then allow us to derive relations between higher-order cumulants. From this recipe, we find the following relation between the two-particle reducible vertex functions

$$F_{k,k',q;i\omega,i\omega',i\nu} = T(k+q,i\omega+i\nu)T(k,i\omega)\,F^d_{k,k',q;i\omega,i\omega',i\nu} \times T(k',i\omega')T(k'+q,i\omega'+i\nu) \quad (37)$$

in real and dual space, where

$$T(k,i\omega) = \frac{G_d(k,i\omega)}{G(k,i\omega)[\Delta(K,i\omega) + \overline{h}_K - h_k]\bar{g}(K,i\omega)} = -[1 + \bar{g}(K,i\omega)\Sigma_d(k,i\omega)]^{-1}. \quad (38)$$

Similar relations hold for many-particle vertex functions. With the help of the two-particle vertex function, we can now express the corresponding susceptibility as $\chi = \chi_0 + \chi_0 F \chi_0$. Since from Eq. (38) it follows that $T(k,i\omega)$ is always finite, a divergence of $\chi$, signaling an instability or phase transition in real space, necessarily corresponds to an instability in the quantity $F^d$ in the dual fermion space. In order to locate the instabilities, it is hence sufficient to search for a divergence of the Bethe-Salpeter equation in the dual space. For the special case when no diagrammatic corrections to the dual self-energy and vertex are taken into account, $T(k,i\omega) = -1$ and both DFDCA and DCA would produce the same phase diagram. In general cases, the DFDCA will produce results more realistic than DCA due to the inclusion of additional long-ranged correlations from the dual fermion lattice diagrammatic calculation.

### III. DUAL FERMION DIAGRAMS

In the DFDCA formalism, the dual fermion Green function is $\mathcal{O}(1/L_c)$[c.f. Eq. (28)], i.e., it acts as the small parameter in the diagrammatic expressions. In addition, in the strong-coupling limit, the Green function is proportional to the hopping $t/U$,[19] so each Green function leg contributes a factor of $\mathcal{O}[(t/U)/L_c]$. In the weak-coupling limit, the Green function remains $\mathcal{O}(1/L_c)$, but the vertices are now small, with the two-body vertex behaving like $\mathcal{O}(U/t)$, the three-body vertex like $\mathcal{O}(U^2)$, and so on. Each two-body diagrammatic insertion, composed of a two-body vertex and two dual fermion Green function legs, then scales like $\mathcal{O}(1/L_c^2)$, with an additional factor of $U$ or $t^2$ in the weak- and strong-coupling limits, respectively. Each three-body diagrammatic insertion, composed of a three-body vertex and three dual fermion Green function legs, scales like $\mathcal{O}(1/L_c^3)$ with additional factors $U^2$ or $t^3$ in the weak- and strong-coupling limits, respectively.

The boundary condition (22) also constraints the diagrammatics. For example, the first-order contribution to the dual self-energy from the two-body interaction is the Hartree-Fock contribution shown in Fig. 2. Since the vertex depends only upon the small cluster $K$, the dual Green function line may be coarse grained. The result is zero by virtue of Eq. (22). Physically, this term must be zero since the Hartree term is already included in the cluster contribution to the self-energy. Therefore the first finite contribution to the dual fermion self-energy comes from the second-order graph, which contains three dual fermion Green function lines. This and all higher-order contributions described by the Schwinger-Dyson equation already are of order $\mathcal{O}(1/L_c^3)$ or smaller. Therefore the fully dressed dual fermion Green function retains the scaling of the bare dual fermion Green function

$$G_d(k,i\omega) \sim \mathcal{O}(1/L_c), \tag{39}$$

as anticipated earlier.

Similarly, the first-order three-body contribution to the dual two-body vertex, also shown in Fig. 2, is zero. To see this, suppose the top leg is labeled by momentum $k = K + \tilde{k}$. Since the remainder of the three-body vertex does not depend upon $\tilde{k}$, we may freely sum over this label. Again, the result is then zero through Eq. (22).

As the cluster size becomes large, the DFDCA cluster problem may be accurately solved using low-order perturbation theory, keeping only the two-body interaction vertex.

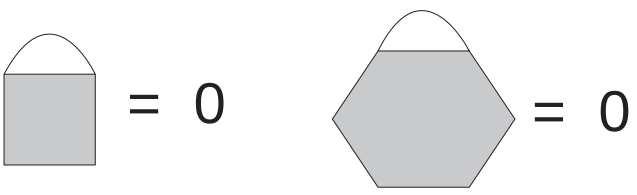


FIG. 2. Lowest-order contributions to the dual fermion self-energy from the two-body interaction (left) and to the two-body interaction from the three-body term (right). Since the bare $n$-body vertices depend only upon the small cluster $K$, the dual Green function line may be coarse grained, and they are therefore zero according to Eq. (22).

As described above, two-body vertex insertion contributes an extra factor of $\mathcal{O}(1/L_c^2)$, while three-body vertex insertion contributes an extra factor of $\mathcal{O}(1/L_c^3)$. It is therefore possible to use standard perturbation theory based on a two-body vertex to solve the dual fermion DCA cluster problem, with an accuracy which turns out to be at least of order $\mathcal{O}(1/L_c^4)$.

For example, simple second-order perturbation theory yields a self-energy $\mathcal{O}(1/L_c^3)$. Two-body corrections, composed of a two-body vertex and two further Green function legs will contribute an extra factor $\mathcal{O}(1/L_c^2)$. The first three-body contribution is the second-order graph composed of one two-body and one three-body vertices. It has four internal Green function legs and is of order $\mathcal{O}(1/L_c^4)$ so that the first three-body correction is smaller than the simple second-order dual fermion self-energy composed of two-body vertices by a factor of $\mathcal{O}(1/L_c)$. Self-consistency, needed to impose the boundary condition (22), is more important for the self-energy than higher-order or three-body contributions.

Generally, the leading nontrival $n$-body ($n \geqslant 3$) vertex contribution to the self-energy is constructed from an $n$-body vertex and an $(n-1)$-body vertex, which are connected by $(2n-2)$ internal legs, as shown in Fig. 3. Thus this contribution scales as $\mathcal{O}(1/L_c^{2n-2})$.

As another example, consider the equation for a transition, in the pairing matrix formalism (see Fig. 4)

$$\Gamma_d \chi_d^0 \Phi = \Phi, \tag{40}$$

where $\Phi$ is the leading eigenvector of the pairing matrix $\Gamma_d \chi_d^0$. A transition is indicated by the corresponding eigenvalue approaching one. To lowest order, the irreducible dual fermion vertex $\Gamma_d \approx \gamma$ is just the bare dual fermion interaction, and the legs in $\chi_d^0$ are not dressed by the dual fermion self-energy. In this case, the transition temperatures of the DCA are reproduced (e.g., see Fig. 5). The lowest order corrections to the DCA come from the second-order corrections to the vertex, which contain two dual fermion Green function legs and are therefore $\mathcal{O}(1/L_c^2)$. The low-order contributions to $\chi_d^0$ are $\chi_d^0 \approx G_d^0(1 + \Sigma_d G_d^0 + \cdots)G_d^0$ and thus the lowest relative correction to $\chi_d^0$ is of order $\mathcal{O}(1/L_c^4)$. Therefore the cross channel second-order corrections to the vertex are more important than the second-order corrections to the self-energy

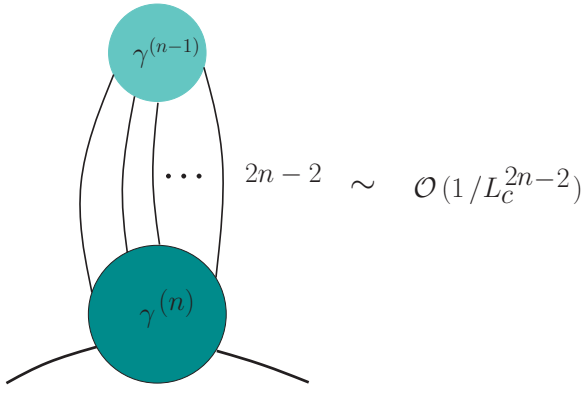


FIG. 3. (Color online) Leading nontrivial $n$-body vertex contribution to the self-energy. It is contructed by one $n$-body vertex and one $(n-1)$-body vertex. Since there are $(2n-2)$ internal legs, this contribution scales as $\mathcal{O}(1/L_c^{2n-2})$.

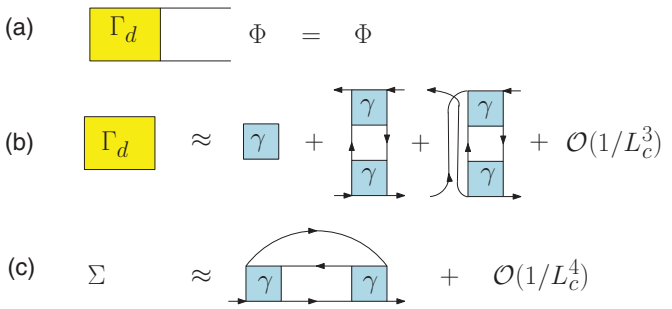


FIG. 4. (Color online) (a) Equation for $T_c$. Transition temperatures on the dual fermion lattice are identical to those calculated on the real lattice. (b) The low-order corrections to the dual fermion irreducible vertex $\Gamma_d$. The second-order terms are of the order $\mathcal{O}(1/L_c^2)$ with corrections $\mathcal{O}(1/L_c^3)$. (c) Contributions to the dual fermion self-energy. It is dominated by the second-order term, which is of the order $\mathcal{O}(1/L_c^3)$ with corrections $\mathcal{O}(1/L_c^4)$. The self-energy adds relative corrections to $\chi_d^0$ of order $\mathcal{O}(1/L_c^4)$ (see the text for the detail), so the most important contributions to the equation for $T_c$ come from the second-order cross channel contributions to $\Gamma_d$.

when the DCA cluster size is large. We note that this is not only true for the DFDCA, but also for the DFDMFA in the strong-coupling limit where the small parameter $t/U$ replaces $1/L_c$. Furthermore, higher-order approximations, such as the ladder approximation, that do not include these cross channel contributions are not appropriate for the solution of the dual fermion lattice in the limit of large DCA cluster size or small $t/U$.

Higher-order approximations like the fluctuation-exchange approximation (FLEX),[20] which include the cross channel contributions to $\Gamma_d$, should on the other hand be quite accurate. In fact, the FLEX contains all two-particle diagrams to third order. The first diagram neglected by the FLEX is composed

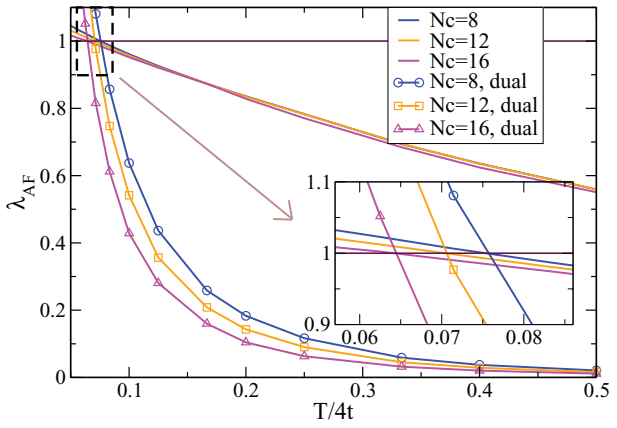


FIG. 5. (Color online) Plots of leading eigenvalues for different cluster sizes for the anti-ferromagnetic channel with $U = 6t$ and filling $\langle n \rangle = 0.95$. Lines without symbols are results from the DCA calculation for clusters with sizes $N_c = 8$, 12, and 16, while lines with symbols are results from the DFDCA calculation without self-energy correction. For the latter, we have used a linear size of the dual fermion lattice as large as several hundreds ($N = L \times L$, $L \sim 200$). The inset is an enlarged view around the transition point. Note that both calculations produce the same transition temperatures as expected.

of one three-body and one two-body vertices and would contribute a correction $\mathcal{O}(1/L_c^4)$ to the self-energy or $\mathcal{O}(1/L_c^3)$ to the vertices.

## IV. RESULTS

In this section, we will present numerical results from a DFDCA calculation, where the interaction expansion continuous-time quantum Monte Carlo method[23] is employed to solve the cluster problem within the DCA calculation. We will restrict the discussion to the two-dimensional Hubbard model on the square lattice with only nearest neighbor hopping. Thus, for half-filling, we expect strong antiferromagnetic correlations, which will drive an antiferromagnetic transition within DCA. In this case, as the Mermin-Wagner theorem prohibits long-range order except at zero temperature, we expect strong renormalization of the Néel temperature $T_N$ from DFDCA.

To check the correctness of our implementation of the DFDCA approach, we first carry out calculations with the correction from the dual fermion lattice turned off. For this trivial case, one expects DFDCA to reproduce the same physics as DCA. Figure 5 displays the leading eigenvalues for different cluster sizes at filling $\langle n \rangle = 0.95$ for the antiferromagnetic channel. Note that for each cluster size, both the DFDCA and the DCA leading eigenvalues cross the line $\lambda = 1$ at the same temperature, which is the mean-field Néel temperature, and that with increasing cluster size, $T_N$ decreases, as expected. It is also interesting to note that the DFDCA provides a sensitive way to monitor the finite-temperature transitions since the DFDCA leading eigenvalues have a steeper slope when crossing the $\lambda = 1$ line.

For the nontrivial DFDCA calculation, we expect to see for a fixed cluster size a reduction of the Néel temperature since correlations beyond the cluster scale are now incorporated by the dual fermion calculation. For the dual fermion lattice, we employ different approximation schemes: the self-consistent second-order perturbation theory (SOPT), FLEX and the parquet approximation (PA).[21] The results are collected in Fig. 6, where the power of DFDCA manifests itself clearly.

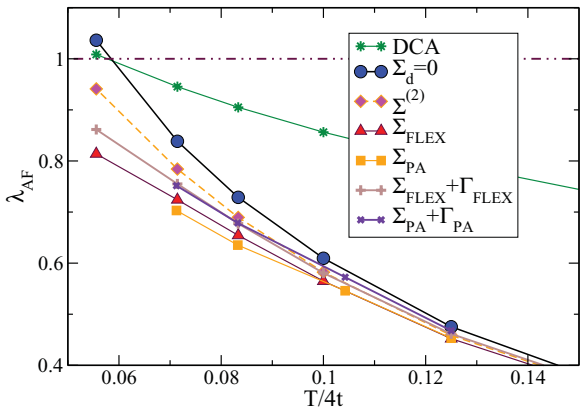


FIG. 6. (Color online) Plots of leading eigenvalues for the antiferromagnetic channel. They are calculated with different approximate methods in the dual fermion lattice. The parameters used are $U = 4t$, $\langle n \rangle = 1$, the DCA cluster of size $N_c = 1$, and the dual fermion lattice of a size $N = 4 \times 4$.

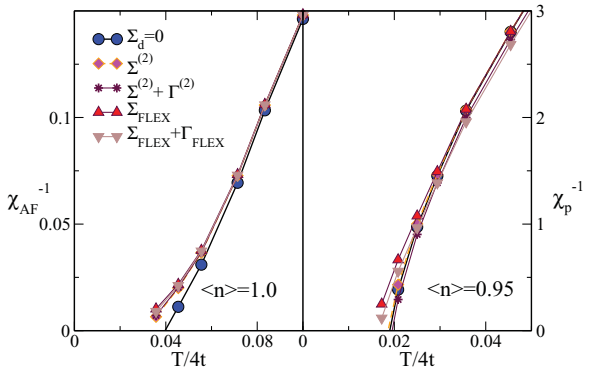


FIG. 7. (Color online) Plots of the inverse antiferromagnetic and $d$-wave pairing susceptibilities calculated with different approximate methods in the dual fermion calculation. The parameters used are $U = 8t$ and $N_c = 4$. The linear dependence of the results with $1/L^2$ (see Fig. 8) is used to extrapolate the $L = \infty$ limit results.

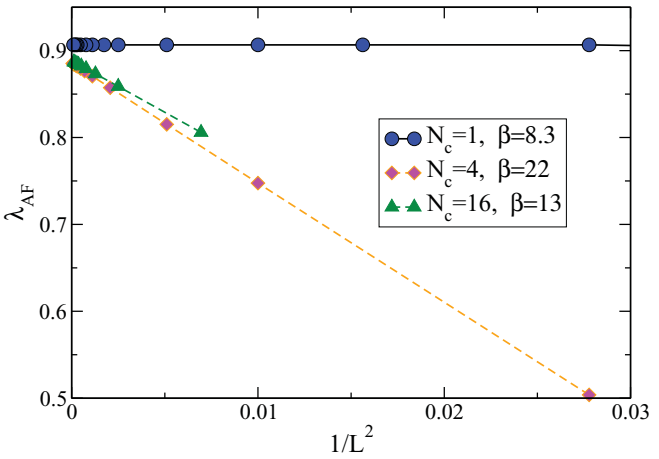


FIG. 8. (Color online) The $L$ dependence of the leading eigenvalue for different DCA clusters. The parameters used are $U = 8t$, $\langle n\rangle = 1$, $\Sigma_{\text{dual}} = 0$, and $\beta = 4t/T$. The nice linear dependence of $1/L^2$ can be readily observed, which is due to the periodic boundary conditions used in the dual fermion calculation.

The simple second-order correction from the self-energy is already able to reduce the Néel temperature by 10%. Taking into account more Feynman diagrams with higher orders, for example by FLEX or PA, continues to reduce the Néel temperature. However, the inclusion of vertex correction tends to increase the Néel temperature again. For example, the eigenvalues labeled $\Sigma_{\text{FLEX}}$ are calculated with a bare dual fermion vertex and FLEX dressed legs, while those labeled $\Sigma_{\text{FLEX}} + \Gamma_{\text{FLEX}}$ are calculated with both FLEX dressed legs and vertex [see (b) and (c) in Fig. 4 for contributions up to second-order in the bare dual fermion vertex $\gamma$].

Up to now, we have only discussed the leading eigenvalues of the vertex function. Of course, the DFDCA also allows to calculate the full susceptibility from the Bethe-Salpeter equation. Two typical results for an $N_c = 2 \times 2$ DCA cluster are shown in Fig. 7, as function of temperature for $U = 8t$. In the left panel, the inverse staggered susceptibility for half filling is displayed, while the right one contains results for the inverse $d$-wave pairing susceptibility at a filling $\langle n\rangle = 0.95$. Due to the heavy computational cost for the parquet calculation, here we only use the SOPT and FLEX in our dual fermion lattice calculation. Although $L_c = 2$ is not really large, the DFDCA is still able to significantly reduce the mean-field Néel and the abnormally large superconducting transition temperatures. It is quite interesting to note, that for the antiferromagnetic channel at half filling, SOPT and FLEX produce similar results, both being different from the DCA results. The effect of vertex correction is small in this case. For the $d$-wave pairing susceptibility at $\langle n\rangle = 0.95$, on the other hand, SOPT in dual space makes almost no difference from the DCA results, but the FLEX tends to significantly reduce the pairing susceptibility. Again, the inclusion of vertex correction has the opposite effect, i.e., it leads to a slight increase of the critical temperatures.

In the derivation of the DFDCA approach, we have assumed that the dual fermion lattice is infinite. However, in practical calculations, the size is limited due to the algebraic increase of the computational cost. This results in some deviations from the infinite size system. Figure 8 shows the $L$ ($N = L \times L$) dependence of the leading eigenvalues for different DCA clusters. The nice linear dependence of the leading eigenvalues on $1/L^2$ can be readily observed. This is due to the periodic boundary conditions used in the dual fermion calculation. This property allows us to reduce the computational cost of our calculation by using two small $L's$ and extrapolating to obtain a rather accurate approximation of the $L = \infty$ result.

## V. DISCUSSION

The dual fermion mapping as discussed in Sec. II is exact, and the approximation is made only when performing the diagrammatic calculation for the dual fermion lattice. Justified by the scaling behavior of the dual fermion Green function, it suffices to consider the two-body term of the interaction and use low-order perturbation theory. Correlations beyond the DCA cluster size are systematically restored through the dual fermion calculation on the lattice. In this sense, the DFDCA can be seen as a diagrammatic expansion around DCA. This is manifested in Figs. 5 and 6 where we see that not including the dual fermion self-energy and vertex corrections reproduces the DCA transition temperature. When these corrections are included, we observe a systematic suppression of the DCA transition temperature resulting in a more realistic value. This is clearly seen in Figs. 6 and 7. Since correlations at intermediate length scale are taken into account by the dual fermion lattice calculation, we can use small clusters in the underlying DCA calculation. As a result, we are able to greatly reduce the adverse effect of the minus sign problem encountered in QMC simulations for larger clusters, and access a wider region of parameter space.

The DFDCA has an additional advantage that it is parameterized by the full (reducible) vertex function calculated on the DCA cluster. Other multiscale methods[11–13] rely upon the calculation of the cluster irreducible or fully irreducible vertices. Our recent numerical experiments show that inverting the Bethe-Salpeter equation to obtain the irreducible vertex, which is also the first step in the calculation of the fully irreducible vertex, fails in some parameter regions, especially

for large $U$ or near half filling. This difficulty is avoided in the DFDCA.

The dual fermion mapping also assumes that the dual fermions are treated on an infinitely large lattice. In practice, however, they are treated on a finite-size lattice. Thanks to the finite-size scaling behavior observed in Fig. 8, finite-size calculations are used to extrapolate to the infinite-size lattice, leading to a reduction of the computational cost in the dual fermion lattice calculation.

Note that in the calculations presented here, we have not performed the full self-consistency where the dual fermion result is used to determine the DCA cluster hybridization that is fed back into the DCA calculation until convergence. However, this first iteration already produces more satisfactory values for the Néel temperature as well as the $d$-wave superconducting transition temperature. We can anticipate that the full self-consistency will further improve the performance of this approach.

With the full self-consistency implemented and tested, we are planning to apply this approach to map out the phase diagram for the two-dimensional (2D) Hubbard model in the hole-doped region. In addition, we are also working on applying this approach to the Falicov-Kimball model and the Anderson disorder model.

## VI. CONCLUSION

We have designed a multiscale many-body approach, the dual fermion dynamical cluster approach (DFDCA), by combining the DCA and the recently introduced dual fermion formalism. The DFDCA uses both single- and two-particle quantities calculated in DCA as the input for the dual fermion calculation. Different self-consistent diagrammatic approximations can be used in the dual fermion lattice, which systematically restores the long-ranged correlation ignored during the DCA calculation.

This approach is a systematic expansion around the DCA calculation. Our numerical experiments show that the zeroth order result ($\Sigma_d = 0$) reproduces the original DCA, and for any nontrivial dual fermion calculation, it is an improvement on the DCA calculation. We applied different self-consistent diagrammatic methods, self-consistent second-order, FLEX, and parquet approximation, on the dual fermion lattice. They all improved the DCA calculation by reducing the mean-field Néel temperature by different amounts. In addition, the abnormally large superconducting transition temperature of the four-site cluster calculation can be reduced by this approach as well.

## ACKNOWLEDGMENTS

We would like to thank A. I. Lichtenstein for useful conversations. This research is supported by DOE SciDAC DE-FC02-06ER25792 (S.X.Y, H.F., K.M.T., and M.J.) and NSF Grants OISE-0952300 (S.X.Y., H.F., and J.M.). This research was supported in part by NSF through TeraGrid resources provided by the National Institute for Computational Sciences under Grant No. TG-DMR100007 and by the high-performance computational resources provided by Louisiana State University (http://www.hpc.lsu.edu).

[1] Y. Kuramoto, Springer Series in Solid State Science Vol. 62, edited by T. Kasuya and T. Saso (Springer, 1985), p. 152.
[2] W. Metzner and D. Vollhardt, Phys. Rev. Lett. **62**, 324 (1989).
[3] E. Müller-Hartmann, Z. Phys. B **74**, 507 (1989).
[4] T. Pruschke, M. Jarrell, and J. K. Freericks, Adv. Phys. **42**, 187 (1995).
[5] A. Georges, G. Kotliar, W. Krauth, and M. J. Rozenberg, Rev. Mod. Phys. **68**, 13 (1996).
[6] G. Kotliar, S. Y. Savrasov, K. Haule, V. S. Oudovenko, O. Parcollet, and C. A. Marianetti, Rev. Mod. Phys. **78**, 865 (2006).
[7] M. H. Hettler, A. N. Tahvildar-Zadeh, M. Jarrell, T. Pruschke, and H. R. Krishnamurthy, Phys. Rev. B **58**, R7475 (1998).
[8] M. H. Hettler, M. Mukherjee, M. Jarrell, and H. R. Krishnamurthy, Phys. Rev. B **61**, 12739 (2000).
[9] M. Jarrell, Th. Maier, C. Huscroft, and S. Moukouri, Phys. Rev. B **64**, 195130 (2001).
[10] G. Kotliar, S. Y. Savrasov, G. Pálsson, and G. Biroli, Phys. Rev. Lett. **87**, 186401 (2001).
[11] A. Toschi, A. A. Katanin, and K. Held, Phys. Rev. B **75**, 045118 (2007).
[12] C. Slezak, M. Jarrell, Th. Maier, and J. Deisz, J. Phys. Condens. Matter **21**, 435604 (2009).
[13] H. Kusunose, J. Phys. Soc. Jpn. **75**, 054713 (2006).
[14] A. N. Rubtsov, M. I. Katsnelson, and A. I. Lichtenstein, Phys. Rev. B **77**, 33101 (2008).
[15] A. N. Rubtsov, M. I. Katsnelson, A. I. Lichtenstein, and A. Georges, Phys. Rev. B **79**, 045133 (2009).
[16] H. Hafermann, G. Li, A. N. Rubtsov, M. I. Katsnelson, A. I. Lichtenstein, and H. Monien, Phys. Rev. Lett. **102**, 206401 (2009).
[17] H. Hafermann, S. Brener, A. N. Rubtsov, M. I. Katsnelson, and A. I. Lichtenstein, JETP Lett. **86**, 677 (2007).
[18] Note that since the interaction is assumed to be local, it is unaffected by coarse graining. Nonlocal interactions however will be coarse grained.
[19] H. Hafermann, *Numerical Approaches to Spatial Correlations in Strongly Interacting Fermion Systems* (Cuvillier Verlag Göttingen, 2010).
[20] N. E. Bickers and D. J. Scalapino, Ann. Phys. **193**, 206 (1989).
[21] S. X. Yang, H. Fotso, J. Liu, T. A. Maier, K. Tomko, E. F. D'Azevedo, R. T. Scalettar, T. Pruschke, and M. Jarrell, Phys. Rev. E **80**, 046706 (2009).
[22] M. Jarrell, Th. Maier, M. H. Hettler, and A. N. Tahvildarzadeh, Europhys. Lett. **56**, 563 (2001).
[23] E. Gull, A. Millis, A. Lichtenstein, A. Rubtsov, M. Troyer, and P. Werner, Rev. Mod. Phys. **83**, 349 (2011).